Influence of Applied Frequency on Thermal Physical Properties of Coatings Prepared on Al and AlSi Alloys by Plasma Electrolytic Oxidation

Guodong Li [1,2], Fei Ma [3], Zhijie Li [3], Yi Xu [1,2], Fangyuan Gao [1,2], Lingyan Guo [3], Jianwei Zhu [1,2], Guang Li [1,2,*] and Yuan Xia [1,2,*]

1 Institute of Mechanics, Chinese Academy of Sciences, Beijing 100190, China; lgd@imech.ac.cn (G.L.); xuyi@imech.ac.cn (Y.X.); gaofangyuan@imech.ac.cn (F.G.); zhujianwei@imech.ac.cn (J.Z.)
2 Center of Materials Science and Optoelectronics Engineering, University of Chinese Academy of Sciences, Beijing 100049, China
3 Weichai Power Co., Ltd., Weifang 261061, China; mafei01@weichai.com (F.M.); lizhij@weichai.com (Z.L.); guoly@weichai.com (L.G.)
* Correspondence: lghit@imech.ac.cn (G.L.); xia@imech.ac.cn (Y.X.)

Abstract: In this study, plasma electrolytic oxidation (PEO) was performed on Al and AlSi substrates using a pulsed direct current (DC) power source. The coating process was carried out in a Na_2SiO_3 electrolyte with the systematic change of pulse frequency (50–1400 Hz). The surface characteristics of the coatings were examined using scanning electron microscopy (SEM). The phase structure was characterized using X-ray diffraction (XRD). A differential scanning calorimeter (DSC) and a laser flash apparatus (LFA) were employed to test heat capacity and heat conductivity, respectively. Results showed that as the discharge frequency increased, the thermal physical properties of Al-PEO and AlSi-PEO coatings changed in different ways. At a high frequency, Al-PEO coatings had low porosity and were closed-pore structured whereas AlSi-PEO coatings had high porosity and large-size open-pore structures could be observed on their surfaces due to concentrated discharges. Based on these findings, it was found that the thermal productivity of coatings is closely correlated with the open-/closed-pore structure instead of porosity. PEO coatings with low heat capacity or low heat conductivity could be obtained with a controlled frequency.

Keywords: PEO; low heat capacity; low heat conductivity; microstructure

1. Introduction

Improvement in the thermal efficiency of internal combustion engines plays a significant role in energy conservation and emission reduction, which is also a major strategy adopted by the energy and power industries of countries across the globe [1–3]. The thermal protection coating technology is one of the critical methods used to increase the thermal efficiency of internal combustion engines. Yttria-stabilized zirconia (YSZ) ceramic coatings have been widely used as thermal insulation coatings in the internal combustion engine sector [4–6], as they have superior properties of low heat conductivity and high fracture toughness, which can dramatically improve the piston top temperature as well as the combustion efficiency.

However, although YSZ ceramic coatings have low heat conductivity, their volumetric heat capacity is relatively high (>2500 kJ/(m^3·K)) [7–9]. A high volumetric heat capacity often causes coatings to store a large amount of heat during insulation and heat the air intake, which can reduce the number of oxygen atoms used for combustion, resulting in incomplete combustion. As a solution to this, coatings with low heat capacity are considered as a feasible way to increase internal combustion efficiency, as their surface temperature can decrease rapidly during the exhaust stroke, which can prevent the coatings from heating the air intake during the intake stroke [10].

At present, most of the research on thermal protection coatings mainly focuses on their low heat conductivity, while only a few research teams have studied how to realize the thermal protection function using low volumetric heat capacity. In 2017, the research team New ACE from Japan [11] designed a new kind of coating with low heat capacity using the plasma spraying method, and its porosity was as high as 60%. However, high porosity will adversely affect the strength of materials, resulting in coating spallation at an early stage. In addition, Kogo et al. [12], from Toyota Motor Corporation, tried to form a multi-porous anodic alumina coating on the surface of the piston chamber of a diesel engine, whose volumetric heat capacity was as low as 1300 kJ/(m$^3\cdot$K) at 500 °C. However, they did not conduct detailed research on the effect of experimental parameters on the thermal property. The PEO technology, as an extension of the aluminum anodization technology, possesses the advantage of in situ growth of high adhesion. In addition, since the heat conductivity of static air is as low as 0.026 W/(m·k), an increase in coating porosity will contribute to an improvement in the thermal insulation performance of coatings. In addition, the spark breakdown characteristic of the PEO technology can give rise to a large number of pores in coatings [13–15]. Therefore, the PEO technology has an inherent advantage when producing coatings with low heat capacity and low heat conductivity.

As PEO coatings are produced based on arc discharge in the liquid phase, their properties are closely related to discharge parameters [16–19]. For instance, research conducted by Clyne [20], from Cambridge University, revealed that coatings with much looser microstructures could be obtained at high frequency. Similarly, Seong et al. [19], from Mokpo National Maritime University, discovered that the microstructures and electrochemical properties of coatings could be dramatically changed by controlling discharge parameters. However, so far, limited studies have been reported on the effect of discharge parameters on heat capacity and heat conductivity of coatings prepared by PEO.

Given the above-mentioned situations, this study aims to explore the influence of different discharge frequencies on the thermal physical properties of coatings produced by PEO. In this study, PEO coatings are prepared on AlSi and Al substrates at different frequencies, and internal relations between coating mechanisms and thermal physical properties are investigated.

2. Materials and Methods

2.1. Preparation of Ceramic Coatings

In the present study, Al and AlSi (ASTM: A0336) with sizes of 15 mm × 15 mm × 5 mm and φ 38 mm × 10 mm were used as substrates, whose corners were perforated for electrical connection. Before experiments, specimen surfaces were polished with 1500 # emery paper. The polished samples were dried after ultrasonic cleaning in propanol and then in ethanol. A Na$_2$SiO$_3$ electrolyte solution was employed in experiments. In the coating process, samples were immersed in the electrolyte and used as an anode, while a stainless-steel material of grade 304 was used as a cathode. The positive terminal of the WHD-30 direct current pulse power supply (Harbin Institute of Technology, Harbin, China) was connected to the anode, and its positive terminal was connected to the cathode. The current density in the anode of all samples was 0.12 A/cm^2. Sample numbers and electrical parameters used in this experiment are exhibited in Table 1.

2.2. Characterization of the Ceramic Coatings

The surface morphology and elemental composition of the coatings were examined by a SUPRA55 scanning electron microscopy (SEM, ZEISS, Oberkochen, German). An X-ray diffractometry (XRD, Rigaku D/Max 2500, Matsumoto, Japan) with CuKα radiation in grazing incidence mode (2°) was used. The maximum power of this XRD was 9 kW, and its working current and voltage were 45 kV and 200 mA, respectively. The coating thickness was measured with an eddy current coating thickness gauge (Huayang HCC-25A, Zhengzhou, China). The thickness was taken as the average value of the thickness measured at 10 different locations of the sample. Before the density testing, samples of

PEO coatings were immersed in an alkaline solution with a high concentration to separate basement membranes to obtain laminated coatings. An electronic balance with a precision of 10^{-5} g (Sartorius, Goettingen, Germany)was employed to measure the quality, and the thickness and area of the stripped coatings were obtained with the microscope and the method of counting pixels, respectively, based on which the coating volume was calculated. Porosity is the ratio of the sum of the pore area in the cross section to its gross area. Before testing, SEM was used to scan the cross-section morphology of the coatings at different angles, which was followed by the calculation of the cross-section porosity of coatings based on the gray-level method (different gray levels between the hole and other regions). A multi-function surface tester (MFT, MFT-4000, Lanzhou, China) developed by the Lanzhou Institute of Chemical Physics of the Chinese Academy of Sciences was employed to measure the roughness of the coatings.

Table 1. Technical parameters of the coatings.

Sample No.	Substrate	Frequency (Hz)	Current Ratio (+/−)	Duty Cycle
A1#		50		
A2#		200		
A3#	Aluminum	600	1/1	45%/50%
A4#		1000		
A5#		1400		
AS1#		50		
AS2#		200		
AS3#	Al-Si alloy (A0336)	600	0.9/1	50%/50%
AS4#		1000		
AS5#		1400		

The specific heat capacity (c) was determined using a differential scanning calorimeter (DSC STA 404C, Netzsch, Selb, Germany). Before testing, coatings were obtained by putting samples in a NaOH solution of 12 g/L for 10 h and the test temperature and the heating rate were set at 300 °C and 10 °C/min, respectively. Ar was used as the purge gas, and the flow rate was 20 mL/min. The DSC curves of the empty crucible, α-Al_2O_3, and coatings were measured using the continuous heating-up scanning method, and the specific heat capacity was calculated based on their quality and the rate of heat flow. The thermal diffusivity (α) of PEO coatings was measured by a laser heat conductivity testing instrument (LAF467 HyperFlash, Selb, Netzsch, German). The data acquisition rate of LAF467 HyperFlash (version: NETZSCH Proteus Software 7.1.0) was up to 2 MHz (mainly reduces the semi-heating signal), and the sampling time could be as low as 1 ms. So it is more accurate for thin film samples; the minimum sample thickness for LAF467 can be as low as 0.01 mm. The heat conductivity (γ) was derived from

$$\gamma = \rho c \alpha = c_v \alpha \tag{1}$$

where α is the thermal diffusivity; ρ and c are the density and the specific heat capacity; respectively; and c_v is the volumetric heat capacity.

3. Results
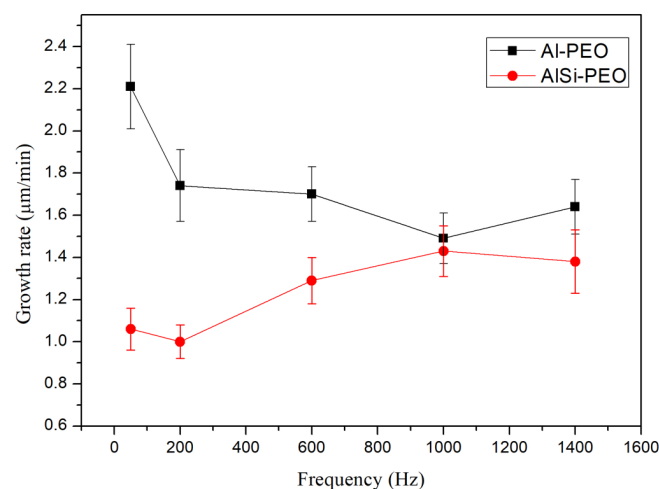
3.1. Growth Rate of PEO Coatings

Figure 1a shows the relationship between the current/voltage and time of samples (anode) in the PEO process, during which the power supply was in bipolar constant voltage mode. At 0–80 s, the current/voltage rose quickly but no plasma discharge was detected. This stage is attributed to anodic oxidation, in which amorphous alumina coatings were formed on the surface [21]. After 80 s, plasma discharge was observed on the surface of the samples, and after 140 s, when the current reached the set value, sustained, stable discharges occurred on the surface while the growth rate of the voltage tended to reduce.

As Figure 1b shows, τ_a in the plot is the anode pulse stage, where discharge breakdown occurs on the surface of samples. τ_c in the plot is the cathode pulse stage, where the voltage of the negative electrode is about 75 V.
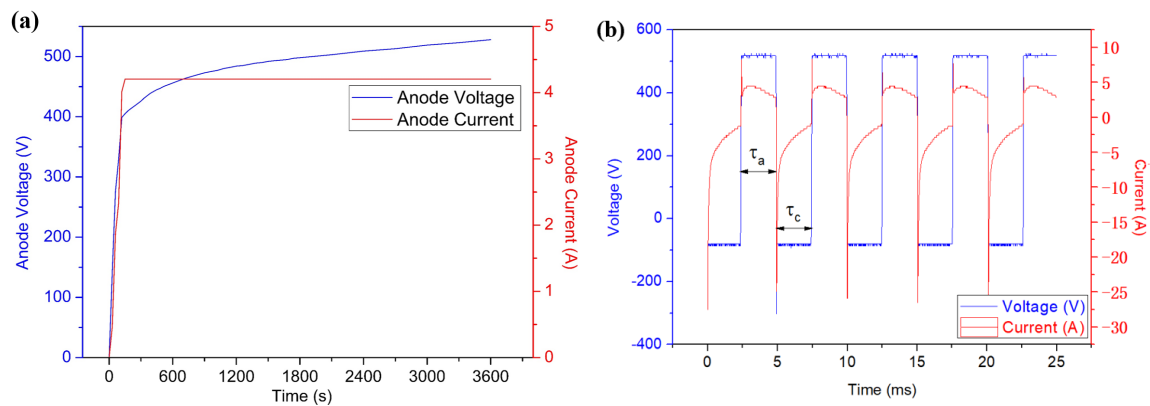
Figure 1. Plots of the PEO treatment of AlSi (200 Hz). (**a**) Voltage– and current–time behaviors; (**b**) waveform.

During the electric discharge machining process, the discharge frequency determines the breakdown in unit time as well as the arcing time of each pulse, thereby affecting the microstructures and properties of coatings. Figure 2 compares the growth rates of different coatings. It can be seen that the growth rates of Al-PEO coatings are related to their looseness (porosity). According to Figure 2, sample A1# had the loosest structure, allowing coatings to have higher growth rates. Sample A4# possessed the highest density, and its growth rate was the lowest correspondingly. Nevertheless, for AlSi-PEO coatings, there was no direct relationship between their growth rates and porosity. For example, although sample AS5# was looser than AS4#, its growth rate tended to decrease slightly. This can be explained by the changes in discharge characteristics induced by Si. During the discharge process, a greater breakdown voltage and breakdown energy are required to spark through Si, which has higher electricity resistivity than Al. At low frequency (50–1000 Hz), the energy provided by a single pulse is sufficient enough to initiate the breakdown effect in ceramic coatings. However, as the frequency increases, the energy of a single pulse decreases so dramatically that it fails to break areas that have large-size bulk Si. It only discharges in weak areas, which reduces the integrity of the coatings produced by plasma electrolytic oxidation.
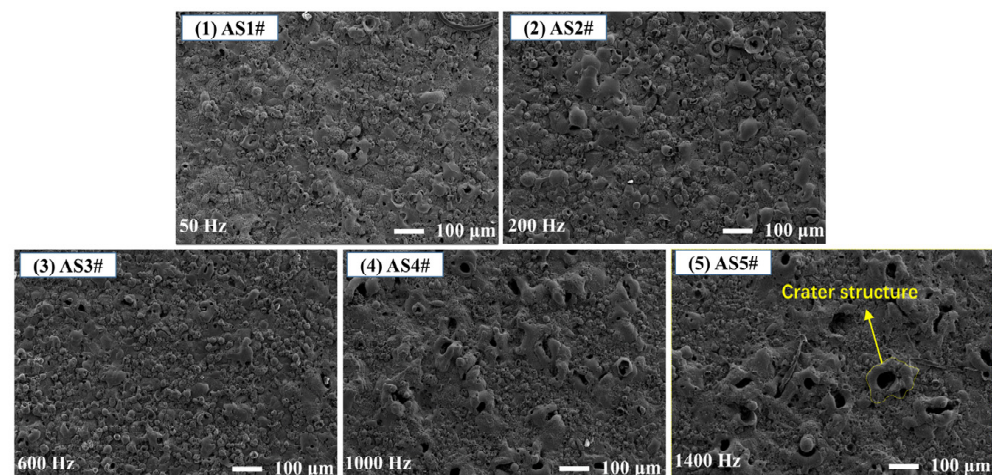

Figure 2. Effects of pulse frequency on the growth rate of coatings.

### 3.2. Morphology and Phase Composition of PEO Coatings

During the electric discharge machining process, the discharge frequency determines the breakdown in the unit time as well as the arcing time of each pulse, affecting the microstructures and properties of coatings. Figures 3 and 4 illustrate surface morphologies of coatings. Figure 5 shows the roughness of all coatings. It can be seen that with frequency increasing, melting materials on the surface of Al-PEO coatings reduced and the surface roughness of the coatings decreased. However, further increase in the frequency (1000–1400 Hz) resulted in a slight increase in the surface roughness (Figure 5). Therefore, compared to Al-PEO coatings, frequency has a more significant effect on the microstructure of AlSi-PEO coatings. According to Figure 4, as the frequency increased, a crater structure, characterized by large-size pores, was observed on the surfaces of sample AS4# and sample AS5#. This is because a further increase in the pulse frequency gives rise to a continuous reduction in single-pulse energy, which fails to penetrate areas with a high thickness in ceramic coatings to allow coating growth to proceed. Concentrated arc discharges take place in weak areas of coatings. As a result, large-size open pores occur on the coating surface due to intense partial discharges. In addition, the surface roughness of the coatings increases with the presence of large-size pores.
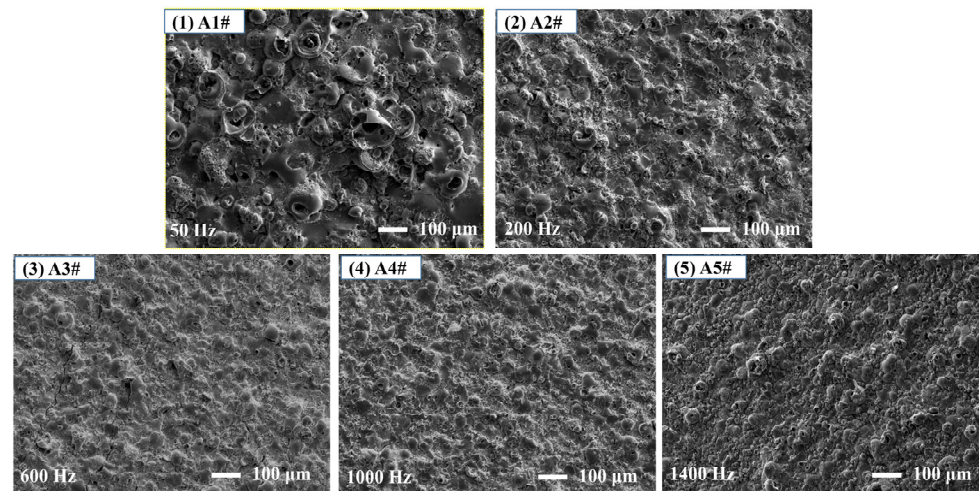
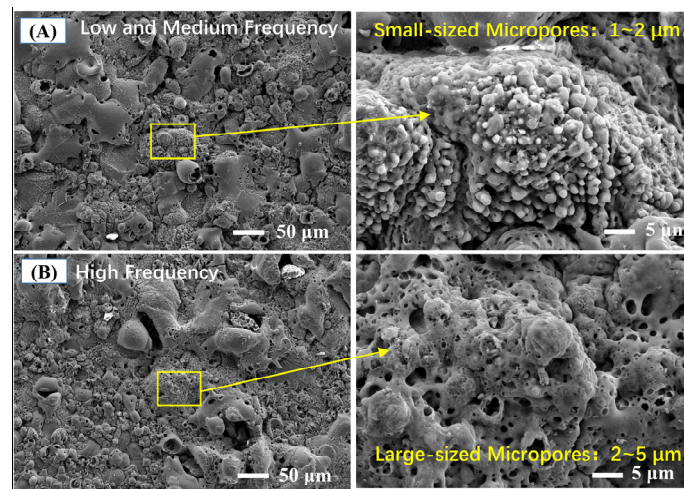**Figure 3.** Surface morphology of Al–PEO coatings (A#) at different pulse frequencies. (**1**) A1#; (**2**) A2#; (**3**) A3#; (**4**) A4#; (**5**) A5#.

Figure 4. Surface morphology of AlSi-PEO coatings (AS#) at different pulse frequencies. (**1**) AS1#; (**2**) AS2#; (**3**) AS3#; (**4**) AS4#; (**5**) AS5#.
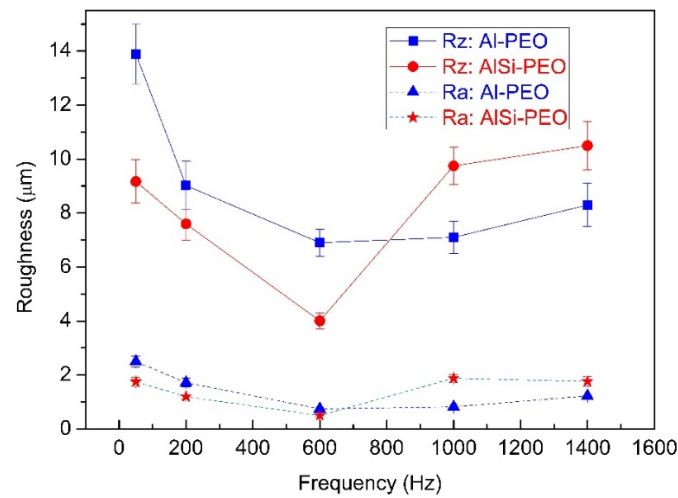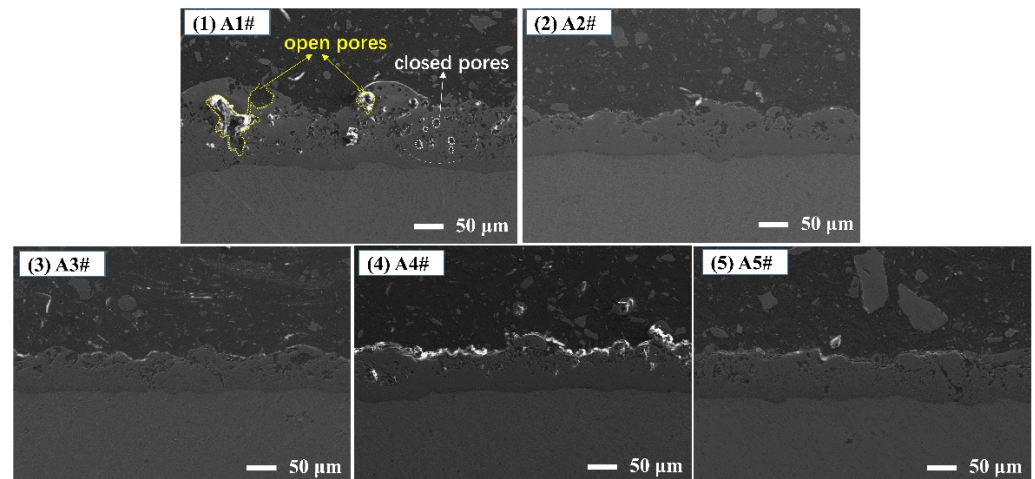
Figure 5. Effects of pulse frequency on the roughness of coatings.

Figure 6 compares partially enlarged views of AlSi-PEO coatings at low and medium frequencies and at high frequency. At low and medium frequencies, small-size micropores (1–2 μm) were observed on the coating surfaces, on which there were large coverage areas formed by melting. However, at high frequency, the micropore size was relatively large (2–5 μm) and the pores had an open structure connected to outside air.


Figure 6. Surface morphology of AlSi-PEO coatings at medium-high frequency. (**A**) Low and medium frequency; (**B**) high frequency.

To further analyze the microstructure and porosity of coatings, the microscopic morphology of coating cross sections was examined (Figure 7) and the changes in Al-PEO coating density and porosity at different frequencies were compared (Figure 8). Hussain et al. [22] categorized discharges during the PEO process into three types. A-type discharges occur on the surface of PEO coatings. Type B refers to strong discharges between PEO coatings and the substrate surface, and during this process, a number of molten oxides eject instantaneously from the discharge channels, which forms a relatively large-size "pancake" structure on the surface of the coatings [23–25]. C-type discharges occur under PEO coatings. In Figures 3 and 7, it can be seen that of all Al-PEO coating samples, A1# exhibited a typical pancake structure induced by B-type discharges. The reasons for this phenomenon will be discussed in Section 4 of this paper.
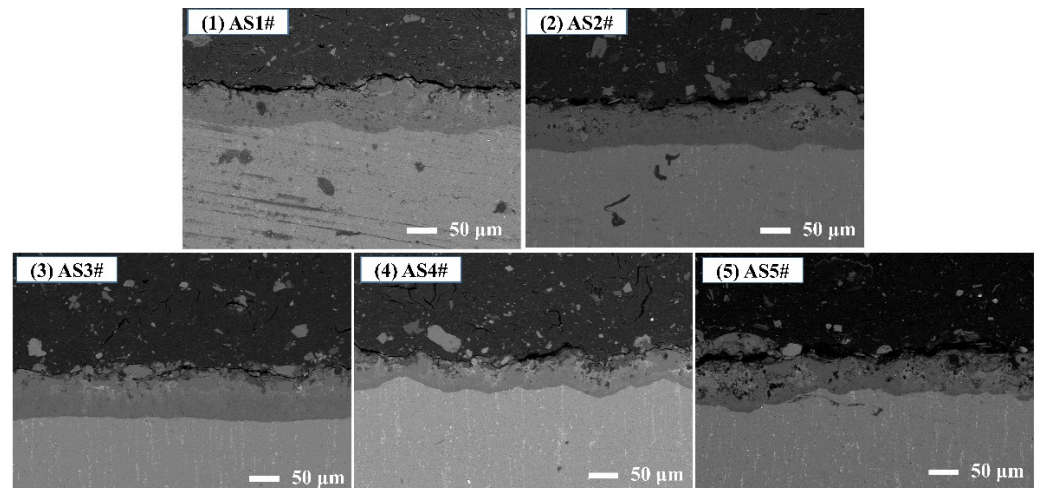
Figure 7. Cross-section morphology of Al-PEO coatings at different pulse frequencies. (**1**) A1#; (**2**) A2#;(**3**) A3#;(**4**) A4#;(**5**) A5#.
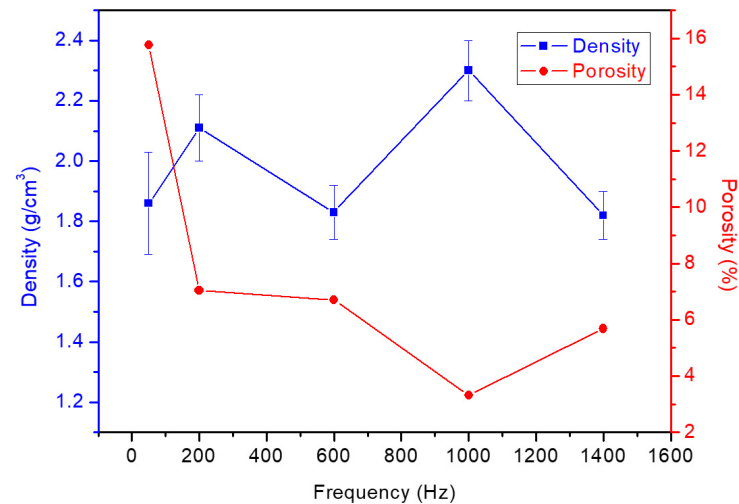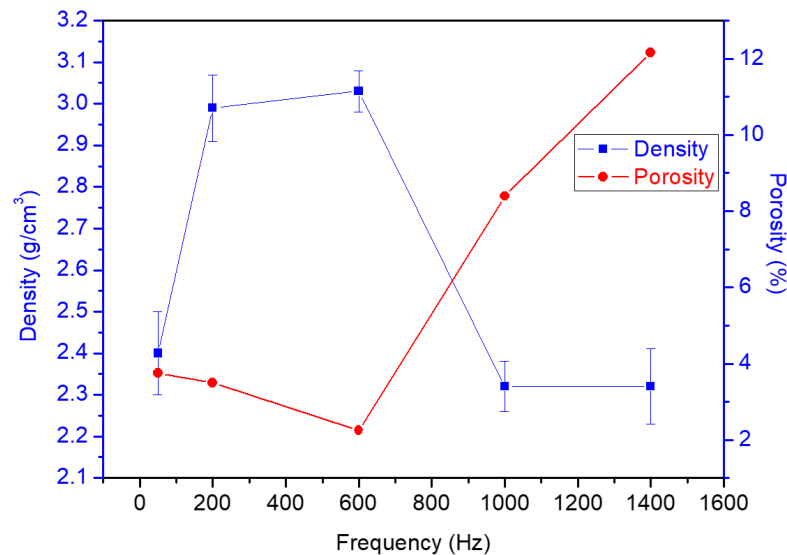

Figure 8. Effects of pulse frequency on the density and porosity of Al-PEO coatings.

From Figure 8, it is evident that for Al-PEO coatings, sample A1# had an obvious porous structure and its porosity tended to decrease as the frequency increased, which is consistent with the pattern of the microscopic morphology observed on coating surfaces. As Figure 8 shows, sample A4# had the lowest porosity, as well as the highest density.

In this section, the cross-section morphologies of AlSi-PEO coatings are compared (Figure 9) and the relationship between coating porosity and density is computed and analyzed (Figure 10). It is evident that the changing pulse frequency can significantly affect the pore structure of coatings, which is similar to the change pattern of surface morphology. At a frequency of 50–600 Hz, with increasing frequency, the porosity of coatings tended to reduce gradually. However, a further increase in the frequency (600–1400 Hz) led to a gradual increase in the coating porosity. In addition, Figure 10 suggests that sample AS3# had the lowest porosity and the highest density, whereas an increase in the porosity of sample AS4# and sample AS5# led to a dramatic reduction in coating density. A comparison between Figures 9 and 10 demonstrates that the change pattern of coating density is not linearly correlated with its porosity, as they are also affected by the compositions of coatings.

Figure 9. Cross-section surface morphology of AlSi-PEO coatings at different pulse frequencies. (**1**) AS1#; (**2**) AS2#; (**3**) AS3#; (**4**) AS4#; (**5**) AS5#.
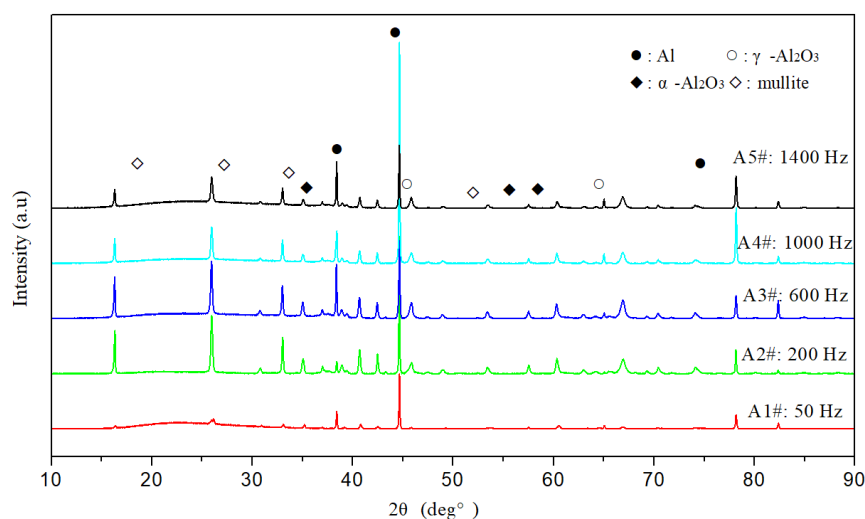

Figure 10. Effects of pulse frequency on the density and porosity of AlSi-PEO coatings.
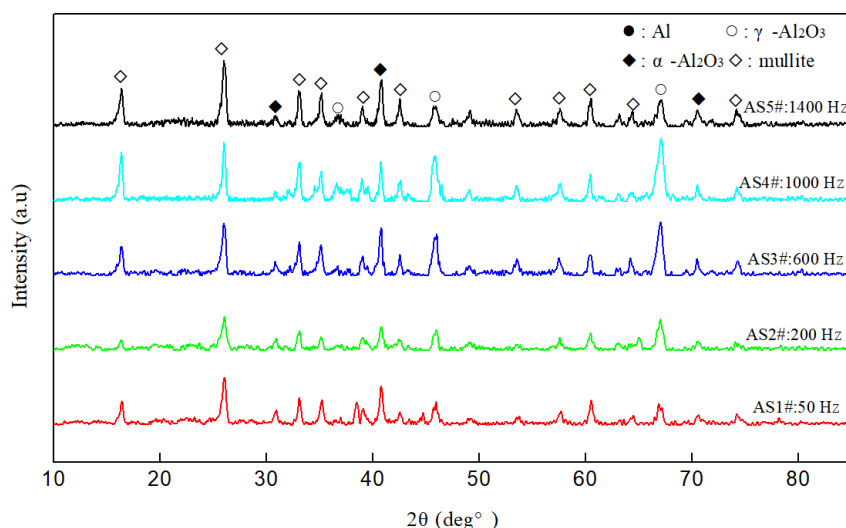
3.3. Phase Structure of PEO Coatings

Figure 11 shows the XRD patterns of Al-PEO coatings. It can be seen that in Na_2SiO_3 solution, Al coatings were mainly composed of α-Al_2O_3, γ-Al_2O_3, $Al_2O_3 \cdot 2SiO_2$, and an amorphous aluminum silicon compound. Sample A1# had many amorphous structures, and the diffraction intensity peaks of the phases were weak. As the pulse frequency increased, the diffraction intensity peaks of α-Al_2O_3 and γ-Al_2O_3 showed a tendency to rise first and then fall. In addition, it is evident that when the pulse frequency was greater than 50 Hz, an obvious mullite phase could be observed in the coatings, and their diffraction peak intensities decreased gradually with a further increase in frequency. This change is consistent with the research reported by Dehnavi et al. [26], who believe that as the pulse frequency rises, an increase in the number of discharges will dissociate more SiO_3^{2-} in the solution from the growing coating surfaces. For Al substrates, since Si in $3Al_2O_3 \cdot 2SiO_2$ mainly comes from SiO_3^{2-} in the solution, the mullite phase in the coatings will decrease gradually due to increasing frequency.

Figure 11. Effects of pulse frequency changes on the phase structure of Al–PEO coatings.

Figure 12 shows the XRD patterns of AlSi-PEO coatings. Similar to Al-PEO coatings, AlSi-PEO coatings were also mainly composed of α-Al_2O_3, γ-Al_2O_3, $3Al_2O_3 \cdot 2SiO_2$, and an amorphous aluminum silicon compound, but the diffraction peak intensities of the phases exhibited different change tendencies. In AlSi-PEO coatings, the Si in $3Al_2O_3 \cdot 2SiO_2$ mainly comes from the AlSi substrates as well as the solution. Unlike Al-PEO coatings, in AlSi-PEO coatings, with rising frequency, the diffraction peak intensity of the mullite phase tends to increase, which can be explained by our previous research. In the AlSi substrate, the edge effect at the interface of the Si phase and the Al phase results from resistivity difference between the two (Al: 2.83×10^{-8} Ωm; Si: 2.3×10^{3} Ωm), because of which the edge becomes the weak area, where discharge breakdown can easily occur [27]. Therefore, a rising pulse frequency leads to an increasing number of breakdowns at the interface of the Si phase and the Al phase in unit time, which causes more Si to melt into coatings, resulting in a higher diffraction peak intensity of the mullite phase.

Figure 12. Effects of pulse frequency changes on the phase structure of AlSi–PEO coatings.

According to XRD change patterns, it is evident that at a pulse frequency of 50–1000 Hz, the diffraction peak intensity of γ-Al_2O_3 in the coatings gradually increased with rising frequency and decreased slightly at a pulse frequency of 1400 Hz. This is because at low frequency, a single pulse has excessive energy and the high temperature resulting from the partial discharge adversely affects the production of the γ-Al_2O_3 phase. However, the

increasing frequency leads to a reduction in single-pulse energy as well as temperature in a small area where discharge occurs, so a γ-Al_2O_3 phase can be observed in the coatings. When the frequency is greater than 1400 Hz, however, coating growth is mullite phase oriented, resulting in a decrease in the diffraction peak intensity of γ-Al_2O_3.

3.4. Heat Capacity of PEO Coatings

From the perspective of coatings, composition and pore structure are two major determinants of their volumetric heat capacity. To better analyze the effect of changing pulse frequencies on the heat capacity of the coatings, Figure 13 compares the relationship between the heat capacities, porosity, and diffraction peak intensities of α-Al_2O_3 and γ-Al_2O_3.
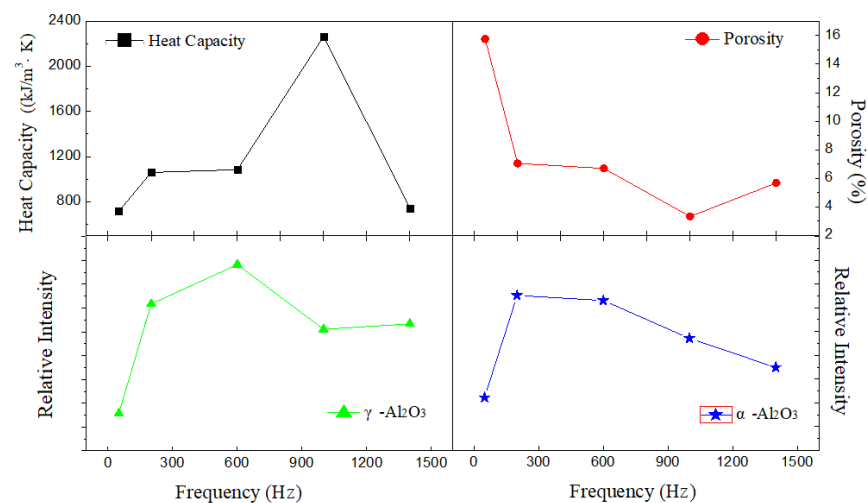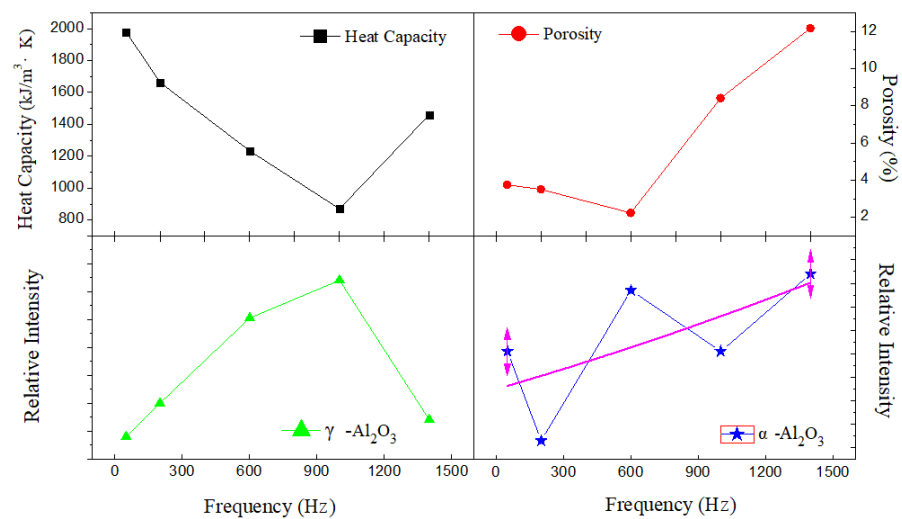

Figure 13. Relationship between the heat capacities, porosity, and phase structures of Al-PEO coatings.

As observed in Figure 13, the volumetric heat capacity of Al-PEO coatings showed a tendency to increase first and then decrease, which is consistent with the changing pattern of porosity. Before the coating process, the volumetric heat capacity of Al is 2422 kJ/m^3·K, which is significantly lower than that after the PEO process. The coatings had the lowest volumetric heat capacity at a pulse frequency of 50 Hz, which can be explained by two reasons. First, sample A1# had the least content of α-Al_2O_3 and γ-Al_2O_3 and was mainly composed of Al_2O_3, with a low heat capacity, which leads to a decrease in the heat capacity. This phenomenon is consistent with the research reported by Clyne [28]. Second, sample A1# was characterized by high porosity and low density. The positive correlation between volumetric heat capacity and density contributes to the low heat capacity of sample A1#. At a pulse frequency of 1000 Hz, the coatings had the highest porosity and their number of micropores decreased dramatically with porosity as low as 3.2%. However, the characteristics of low porosity and high density are the main causes of the highest volumetric heat capacity of the coatings.

Figure 14 illustrates the relationship between the volumetric heat capacity, porosity, and phase structure of AlSi-PEO coatings. Similar to the Al substrate, the heat conductivity of AlSi-PEO coatings (2349 kJ/m^3·K) was dramatically lower than that of the AlSi substrate. It can be seen that sample AS4# had the lowest volumetric heat capacity, which mainly resulted from the compositions and porosity of the coatings. First, at 300 °C, since the heat capacity of the γ-Al_2O_3 phase is lower than that of the α-Al_2O_3 phase, the lower the volumetric heat capacity, the weaker the intensity of the γ-Al_2O_3 diffraction peak with a moderate level of crystallinity in coatings. As for AlSi-PEO coatings, sample AS4# had the highest peak intensity. Second, the high porosity and low density of sample AS4# also contribute to its low heat capacity. Similarly, the high volumetric heat capacity of AS1# is attributed to its low porosity as well as the lowest intensity of the γ-Al_2O_3 diffraction peak.

To sum up, the changing pattern of the volumetric heat capacity of AlSi-PEO coatings is not exactly the same as that of their porosity; instead, it is affected by changes in composition.

Figure 14. Relationship between heat capacities, porosity, and phase structures of AlSi-PEO coatings.

3.5. Heat Conductivity Coefficient of PEO Coatings

Table 2 shows the thermal diffusivity α and heat conductivity γ of substrates and coating samples, from which it can be concluded that the PEO process dramatically reduced the thermal diffusivity and heat conductivity of materials. According to Table 2, the AlSi alloy had lower thermal diffusivity α and heat conductivity γ than Al, which is attributed to the addition of the Si element to the alloy. This result is consistent with the research conducted by Zhang et al. [29], who found that an increase in Si in the AlSi alloy leads to a decrease in thermal diffusivity α and heat conductivity. Sample A5# had the lowest heat conductivity, which is attributed to its low thermal diffusivity and relatively low volumetric heat capacity. From the perspective of microstructure, the low heat conductivity of sample A5# mainly results from a large number of closed pores in coatings. As Figure 7 shows, there were a number of closed pores in coatings, which store trace gases during the formation, forming a large quantity of micron-size closed cells. It is well known that the heat conductivity of static air is as low as 0.023 W/(m·K), so such closed pores lead to a dramatic reduction in the thermal diffusivity and heat conductivity of coatings.

Table 2. Thermal diffusivity (α) and heat conductivity (γ) of samples.

Thermal Properties	Substrate	Frequency (Hz)					Untreated Material
		50	200	600	1000	1400	
α (mm^2/s)	Al	0.394	0.792	0.506	0.321	0.143	85.60
	AlSi	0.102	0.068	0.132	0.220	0.215	70.10
γ (W/mK)	Al	0.281	0.839	0.5486	0.7277	0.106	237.50
	AlSi	0.202	0.113	0.163	0.191	0.314	117.20

A comparison betwee sample A1# and sample A5# suggested that both coatings had low heat conductivity. Although sample A1# had higher porosity, its heat conductivity was higher than that of sample A5#. This is because large-size open pores in coatings are connected to outside air, which enhances the thermal convection. As a result, sample A5# had higher thermal diffusivity, resulting in the higher heat conductivity of sample A5#.

The thermal diffusivity α and heat conductivity γ of Al-Si PEO coatings showed a tendency to fall first and then rise. Sample AS2# had low thermal diffusivity and heat

conductivity, which resulted from the closed pores in the coating, similar to Al-PEO coatings. Similarly, although sample AS4# and sample AS5# had high porosity and low densities, a large number of open, large-size pores inside led to a dramatic increase in the thermal diffusivity of the coatings.

4. Discussion

The above-mentioned data and results show that frequency changes can have effects on the microstructures, mechanisms, and thermal physical properties of PEO coatings. The following section will discuss changes in the property of coatings prepared on different substrates at high and low frequencies.

At different frequencies, the difference between the Al substrate and the AlSi substrate in discharge mode gives rise to a change in the pore structure. During the growth process of a PEO coating on an Al substrate, since the electric field is uniform due to the homogeneity of the substrate, the increasing frequency will result in a reduction in the single-pulse energy as well as an increase of penetrations. This kind of low-energy discharge can cause an increased number of melting zones but a reduction in size, while forming a large quantity of small-size closed pores (see Figure 7). This is consistent with the research reported by Sobolev et al. [23,24], as at a low frequency (A1#), the long duration of each pulse severely heats up the coating, while B-type discharges become dominant, resulting in a large number of open-structured pores on the surface (see Figure 3). However, with frequency increasing, the pulse energy tends to reduce gradually, which allows A-type discharges and C-type discharges to be dominant, leading to a decrease in the porosity. Therefore, with a rise in the frequency, the roughness and porosity of Al–PEO coatings tend to decrease gradually.

Unlike an Al substrate, an AlSi substrate demonstrates a different discharge mechanism. Experiments have demonstrated that at a frequency of 50–600 Hz, A-type discharges and C-type discharges tend to be dominant with the rising frequency, which is attributed to the reduction in single-pulse energy. Nevertheless, a further rise in frequency results in a sudden increase in porosity, which is affected by the Si element in the alloy. First, the AlSi substrate contains a large number of bulk Si phases of different sizes. Due to the difference in the electricity resistivity between Al and Si, the edge effect and the electric field concentration can be easily induced at the interface of the Al phase and the Si phase. Discharge breakdown most likely occurs when the electric field strength is higher than the breakdown voltage of the coating thickness (this phenomenon has been studied in detail in our previous research [27]). During the growth of AlSi-PEO coatings, with the increase in coating thickness, it requires higher breakdown energy to allow the micro-arc oxidation to proceed. However, as the increasing frequency causes a reduction in single-pulse energy, the electric arc concentrated discharges often take place in weak areas such as the interface of the Al phase and the Si phase. The continuous concentrated discharges produce large-size open pores in coatings at a high frequency. Second, discharge breakdown can produce an instantaneous high temperature that is higher than the melting point of Si (~1685 K), SiO_x (<2000 K), Al (~930 K), and Al_2O_3 (~2300 K). This enables materials around the electric melting pool to mix together in the state for melting, forming the Al_2O_3 phase, the SiO_x phase, and the Al-Si-O phase. Since the melting point of the SiO_x phase and the Al-Si-O phase is lower than that of Al_2O_3 phase, the surrounding areas of bulk Si phase are easier to penetrate and concentrated discharge will be induced. This can also explain why the size of pores on AlSi-PEO coatings increases with the rising frequency (increased penetrations).

The analysis reveals that the pore structure characterized by the coatings can reduce their heat capacity and heat conductivity and different pore morphologies have different impacts on both properties. These air-filled closed pores can reduce the heat conductivity of the coatings, thereby decreasing their heat capacity, which is consistent with the research reported by Professor Clyne, from the University of Cambridge. In his research, Clyne [20] investigated the effect of loose and porous layers of PEO coatings on their heat conductivity and found that more air could occupy the pores during the heat transfer process,

thus decreasing the heat conductivity. However, open pores have a different influence mechanism. Since the pores are connected to the outside air, the thermal convection in the coatings can be enhanced, which leads to increased heat conductivity and heat capacity. However, according Equation (1), the heat conductivity of the coatings with an open-pore structure can be indirectly decreased through a reduction in coating density.

5. Summary

The following conclusions can be drawn from this work, which examines the effects of different pulse frequencies on the structure and thermal physical properties of Al-PEO and AlSi-PEO coatings.

1. Coatings produced on Al and AlSi substrates at changing frequencies show different growth patterns. With an increasing frequency, both the growth rate and the porosity of the Al-PEO coatings tend to decrease and a large number of closed-pore structures can be observed in the coatings. However, the growth rate and porosity of the AlSi–PEO coatings have a tendency to increase with rising frequency and many open-pore structures occur in the coatings. This is mainly attributed to the concentrated discharge induced the by Si phase with low impedance.
2. The mullite phase in the Al-PEO coatings disappears with a rising frequency. This is because the Si phase in the Al-PEO coatings mainly comes from the Na_2SiO_3 electrolyte solution and an increase in frequency will dissociate more SiO_3 from the coating surfaces. However, the mullite phase in the Al-PEO coatings tends to increase as the frequency rises. This is because the AlSi substrate contains a large amount of Si and a reduction in the single-pulse energy can enhance the edge effect produced during bulk Si discharge, making more Si elements enter the coatings and increasing the mullite phase.
3. The pore morphology and the quantity of pores in coatings have different impacts on the heat capacity and the heat conductivity. When Al-PEO coatings are prepared at a high frequency and AlSi-PEO coatings at a low frequency, concentrated discharges occur and a large quantity of small-size closed pores are observed in coatings, which leads to a dramatic reduction in the heat capacity and the thermal diffusivity. At a high frequency, a quantity of open pores occurs in AlSi-PEO coatings (e.g., AS5#), which enhances the thermal convection in coatings, leading to increased thermal diffusivity. However, an excessive number of or oversized open pores (e.g., A1#) often results in a decrease in the coating density, which can reduce the volumetric heat capacity of the coatings, thereby indirectly decreasing the heat conductivity.

References

1. Birtok-Băneasă, C.; Rațiu, S.; Puțan, V.; Josan, A. Study of materials used for the thermal protection of the intake system for internal combustion engines. *IOP Conf. Ser. Mater. Sci. Eng.* **2018**, *294*, 012006. [CrossRef]
2. Ma, T.; Chen, D.; Wang, H.; Yao, M.; Xu, A. Influence of thermal barrier coating on partially premixed combustion in internal combustion engine. *Fuel* **2021**, *303*, 121259. [CrossRef]
3. Dhomne, S.; Mahalle, A.M. Thermal barrier coating materials for SI engine. *J. Mater. Res. Technol.* **2019**, *8*, 1532–1537. [CrossRef]
4. Chen, D.; Wang, Q.; Liu, Y.; Ning, X. Microstructure, thermal characteristics, and thermal cycling behavior of the ternary rare earth oxides (La_2O_3, Gd_2O_3, and Yb_2O_3) co-doped YSZ coatings. *Surf. Coat. Technol.* **2020**, *403*, 126387. [CrossRef]
5. Thibblin, A.; Jonsson, S.; Olofsson, U. Influence of microstructure on thermal cycling lifetime and thermal insulation properties of yttria-stabilized zirconia thermal barrier coatings for diesel engine applications. *Surf. Coat. Technol.* **2018**, *350*, 1–11. [CrossRef]
6. Yao, M.; Ma, T.; Wang, H.; Zheng, Z.; Liu, H.; Zhang, Y. A theoretical study on the effects of thermal barrier coating on diesel engine combustion and emission characteristics. *Energy* **2018**, *162*, 744–752. [CrossRef]
7. Song, X.; Xie, M.; Zhou, F.; Jia, G.; Hao, X.; An, S. High-temperature thermal properties of yttria fully stabilized zirconia ceramics. *J. Rare Earths* **2011**, *29*, 155–159. [CrossRef]
8. Sokołowski, P.; Björklund, S.; Musalek, R.; Candidato, R.T.; Pawlowski, L.; Nait-Ali, B.; Smith, D. Thermophysical properties of YSZ and YCeSZ suspension plasma sprayed coatings having different microstructures. *Surf. Coat. Technol.* **2017**, *318*, 28–38. [CrossRef]
9. Kirchheim, R. Incubation time for flash sintering as caused by internal reactions, exemplified for yttria stabilized zirconia. *Acta Mater.* **2019**, *175*, 361–375. [CrossRef]
10. Wakisaka, Y.; Inayoshi, M.; Fukui, K.; Kosaka, H.; Hotta, Y.; Kawaguchi, A.; Takada, N. Reduction of heat loss and improvement of thermal efficiency by application of "temperature swing" insulation to direct-injection diesel engines. *SAE Int. J. Engines.* **2016**, *9*, 1449–1459. [CrossRef]
11. Uchida, N.; Osada, H. A new piston insulation concept for heavy-duty diesel engines to reduce heat loss from the wall. *SAE Int. J. Engines.* **2017**, *10*, 2565–2574. [CrossRef]
12. Kogo, T.; Hamamura, Y.; Nakatani, K.; Toda, T.; Kawaguchi, A.; Shoji, A. high efficiency diesel engine with low heat loss combustion concept-Toyota's inline 4-cylinder 2.8-liter estec 1GD-FTV engine. *SAE World Congr. Exhib.* **2016**, *1*, 1–10.
13. Rudnev, V.S.; Lukiyanchuk, I.V.; Adigamova, M.V.; Morozova, V.P.; Tkachenko, I.A. The effect of nanocrystallites in the pores of PEO coatings on their magnetic properties. *Surf. Coat. Technol.* **2015**, *269*, 23–29. [CrossRef]
14. Zhu, L.; Qiu, J.; Chen, J.; Zhang, W.; Chen, Z.; Zhang, T.; Wang, F. Microstructure and corrosion resistance of the PEO coating on extruded Al6Cu alloy. *Surf. Coat. Technol.* **2019**, *369*, 116–126. [CrossRef]
15. Troughton, S.C.; Nominé, A.; Dean, J.; Clyne, T.W. Effect of individual discharge cascades on the microstructure of plasma electrolytic oxidation coatings. *Appl. Surf. Sci.* **2016**, *389*, 260–269. [CrossRef]
16. Rogov, A.B.; Shayapov, V.R. The role of cathodic current in PEO of aluminum: Influence of cationic electrolyte composition on the transient current-voltage curves and the discharges optical emission spectra. *Appl. Surf. Sci.* **2017**, *394*, 323–332. [CrossRef]
17. Tillous, K.; Toll-Duchanoy, T.; Bauer-Grosse, E.; Hericher, L.; Geandier, G. Microstructure and phase composition of microarc oxidation surface layers formed on aluminium and its alloys 2214-T6 and 7050-T74. *Surf. Coat. Technol.* **2009**, *203*, 2969–2973. [CrossRef]
18. Troughton, S.C.; Clyne, T.W. Cathodic discharges during high frequency plasma electrolytic oxidation. *Surf. Coat. Technol.* **2018**, *352*, 591–599. [CrossRef]
19. Lee, J.-H.; Jung, K.-H.; Kim, S.-J. Characterization of ceramic oxide coatings prepared by plasma electrolytic oxidation using pulsed direct current with different duty ratio and frequency. *Appl. Surf. Sci.* **2020**, *516*, 146049. [CrossRef]
20. Curran, J.A.; Kalkancı, H.; Magurova, Y.; Clyne, T.W. Mullite-rich plasma electrolytic oxide coatings for thermal barrier applications. *Surf. Coat. Technol.* **2007**, *201*, 8683–8687. [CrossRef]
21. Chang, L. Growth regularity of ceramic coating on magnesium alloy by plasma electrolytic oxidation. *J. Alloys Compd.* **2009**, *468*, 462–465. [CrossRef]
22. Hussein, R.O.; Nie, X.; Northwood, D.O.; Yerokhin, A.; Matthews, A. Spectroscopic study of electrolytic plasma and discharging behaviour during the plasma electrolytic oxidation (PEO) process. *J. Phys. D Appl. Phys.* **2010**, *43*, 105203. [CrossRef]
23. Sobolev, A.; Peretz, T.; Borodianskiy, K. Fabrication and characterization of ceramic coating on Al7075 alloy by plasma electrolytic oxidation in molten salt. *Coatings* **2020**, *10*, 993. [CrossRef]
24. Sobolev, A.; Peretz, T.; Borodianskiy, K. Synthesis and growth mechanism of ceramic coatings on an Al-Cu alloy using plasma electrolytic oxidation in molten salt. *J. Alloys Compd.* **2021**, *869*, 159309. [CrossRef]
25. Fatkullin, A.R.; Parfenov, E.V.; Yerokhin, A. Equivalent circuit modelling for pulsed bipolar plasma electrolytic oxidation process. *Int. J. Inf. Electron. Eng.* **2015**, *5*, 63. [CrossRef]
26. Dehnavi, V.; Luan, B.L.; Shoesmith, D.W.; Liu, X.Y.; Rohani, S. Effect of duty cycle and applied current frequency on plasma electrolytic oxidation (PEO) coating growth behavior. *Surf. Coat. Technol.* **2013**, *226*, 100–107. [CrossRef]
27. Xu, F.; Xia, Y.; Li, G. The mechanism of PEO process on Al-Si alloys with the bulk primary silicon. *Appl. Surf. Sci.* **2009**, *255*, 9531–9538. [CrossRef]

28. Curran, J.A.; Clyne, T.W. The thermal conductivity of plasma electrolytic oxide coatings on aluminium and magnesium. *Surf. Coat. Technol.* **2005**, *199*, 177–183. [CrossRef]

29. Zhang, C.; Du, Y.; Liu, S.; Liu, Y.; Sundman, B. Thermal conductivity of Al-Cu-Mg-Si alloys: Experimental measurement and CALPHAD modeling. *Thermochim. Acta* **2016**, *635*, 8–16. [CrossRef]